Hardware and physical integration guideline PCR Sensors A111 & A121

User Guide

Hardware and physical integration guideline PCR sensors A111 & A121

User Guide

Author: Acconeer

Version 1.7: 2024-02-07

Acconeer AB

Table of Contents

1 Introduction

Achieving optimal performance with Acconeer radar sensors is relying on a correct physical integration of the sensor into the customer product. This is especially true for use cases that push the limits for what the sensor can do. A correct integration could give you that extra few degrees in field of view or the extra meter in range that becomes the difference between ok and excellent.

This document aims to provide general guidelines for making a hardware design with the Acconeer A121 and A111 radar sensors. We will provide the essential guidelines to ensure good electrical integration as well as electromagnetic integration. Including PCB design, use of lenses and integration into a radome.

2 Electrical integration

2.1 A111 Power

The A111 radar sensor is powered by 1.8 V and all the control signals, and the SPI interface are 1.8 V pins. It must therefore be ensured that all host MCU pins connected to the A111 are at 1.8 V. If this is not the case, level-shifters must be used in between the A111 and the host MCU.

As mentioned in the power consumption summary of the A111 datasheet, the A111 typically consumes 66 µA when the ENABLE pin is set low. If the leakage current is to be even further reduced, the power to the A111 must be switched off. It can be achieved either by using a low-leakage power regulator with an enable/disable function (if 1.8 V is not available in the system) or a low-leakage power switch in between the two 1.8 V domains. In both cases, a control signal, PMU_ENABLE, is needed. See Figure 2 for details.

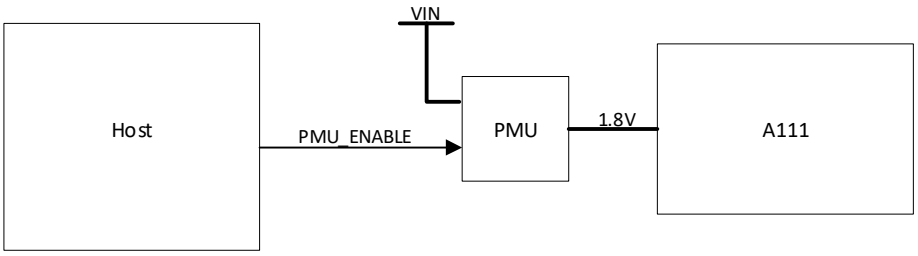

Figure 1. Block diagram of how to connect a Power Management Unit for controlling the 1.8 V to the A111.

If the power to the A111 is switched off in between sweeps it is important that the control signals and SPI interface are pulled low during this time, otherwise reverse leakage will occur via the ESD diodes in the A111. If it is not possible to set the SPI interface in such a state (either via SW or by configuring any level-shifters that might be used in the design), the problem can be solved by adding a power switch only to VIO1 and VIO2. This way the leakage will be significantly lower than 66 µA, but the control signals and SPI interface of A111 will still be supplied by 1.8 V and thus no reverse leakage will occur. See Figure 2 for details. The Acconeer High Performance Module shows how to integrate a power switch into the design, refer to the XM112 datasheet, available on the Acconeer Developer page [1].

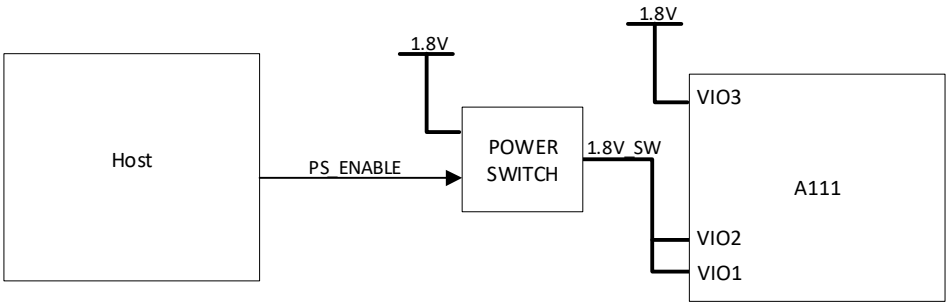

Figure 2. An example of how to connect a power switch to reduce the leakage current when A111 is powered off.

2.2 A121 Power

The A121 radar sensor needs 1.8 V input voltage to the RX, TX and VDIG power domains. The A121 VIO power domain can be powered by either 1.8 V or 3.3 V. To avoid stressing the A121 and to

optimize the current consumption, the VIO on A121 should be equal to the I/O voltage on the host MCU that controls it. The A121 power consumption when the ENABLE pin is low is < 1 µA and there is thus no need for a power switch as is the case for A111.

If the power to the A121 is switched off in between radar sweeps it is important that the control signals and SPI interface are pulled low during this time, otherwise reverse leakage will occur via the ESD diodes in the A121.

2.3 Choosing a 1.8 V power regulator for A111/A121

When the A111/A121 radar sensors transfer from the “SLEEP” state to the “MEASURE” state, there is an abrupt change in current consumption from ~3 mA to ~75 mA on the 1.8 V power domain. It must be ensured that the power regulator used to supply the A111/A121 has a load transient response that handles this change in current without the output voltage dropping below the minimum operating supply voltage of A111/A121. For details regarding the power consumption of A111 and A121, refer to the datasheet of the respective product [2] [3].

2.4 SPI Interface

To ensure good signal integrity for the SPI bus, it is recommended to keep the SPI traces as short as possible with an adjacent ground plane. Place a ground via close to the signal via when changing layers to maintain a constant trace impedance. Impedance matching of the SPI bus is usually not needed as the trace lengths are electrically short for low drive strength configurations.

2.5 Hardware schematics design checklist

1. Does the selected crystal fulfill the load conditions according to the A111/A121 datasheet [2] [3]?
2. Have you connected all ground balls on the package?
3. Is the ground plane size based on Figure 5?
4. Are the decoupling capacitors placed according to the guidelines in chapter 3.3.2?
5. Have you chosen your power regulator based on the information in chapter 2.3?
6. Is the power supply and SPI interface routed with an adjacent ground plane?
7. Have you placed nearby ground vias to your signal and power supply vias?

3 Electromagnetic Integration

The A111 and A121 pulsed coherent radar sensors are fully integrated 60 GHz radar sensors with integrated transmitter and receiver antennas. The Tx and Rx antennas are of folded-dipole type and the E-plane and H-planes are indicated in Figure 3. The RLG patterns can be found in each datasheet, see [2] and [3].

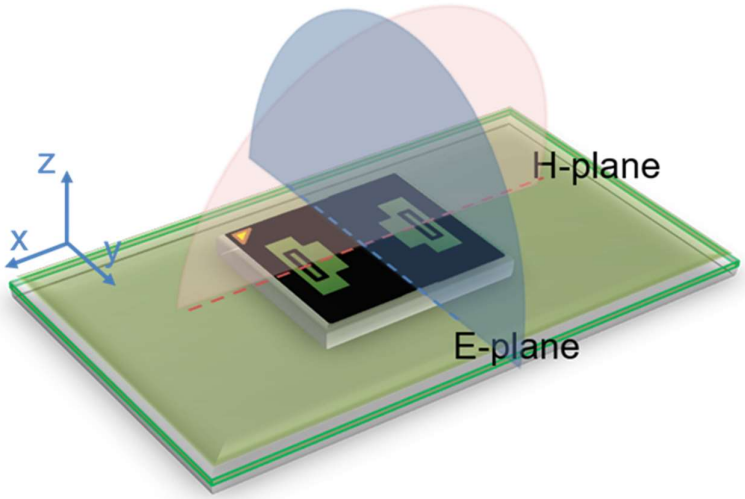

Figure 3. Sensor mounted on a printed circuit board (PCB). E-plane and H-plane are highlighted with blue and red color, respectively.

3.1 Radar loop equation

Consider a signal transmitted through free space to a radar target located at distance R from the radar. Assume there are no obstructions between the radar and the radar target, and the signal propagates along a straight line between the two. The channel model associated with this transmission is called a line-of-sight (LOS) channel. For the LOS channel, the corresponding received reflected power from a radar target, i.e. the signal to noise ratio (SNR), can be defined as

$$SNR = C\sigma\gamma\frac{1}{R^4}, \quad (1)$$

where R is the distance of the radar to the target, C is the radar loop gain, including both the transmitter and receiver chain (two-ways signal path), σ is the Radar Cross Section (RCS) of the scattering object and γ determines the reflected power of the object's material. RCS depends on the size and shape of the scattering object. Moreover, SNR depends on the sensor profile setting. A comprehensive explanation of the sensor profiles can be found in the Acconeer's Radar Handbook" [4].

3.2 Radar loop gain pattern

When characterizing the gain, we refer to the radar loop gain defined in the radar equation section. Figure 4 shows the radar setup configuration for the radar loop radiation pattern measurement. The

reflector which in this case is a circular trihedral corner is located at the far-field distance from the sensor. The far-field distance can be determined by the aperture of the sensor and the radar target.

$$R_{\text{farfield}} > \frac{2A^2}{\lambda} \quad (2)$$

where A is the largest dimension of either the sensor or the radar target. Far-field is the region where the radiation pattern shape does not change with the distance. However, the radar works below the far-field distance with different characteristic than the far-field region with radiation pattern dependency on the distance.

The service “Sparse IQ” (A121) or the “Envelope detector” (A111) can be used to collect the reflected signal at the fixed distance from the radar target for different rotation angles. The figure of merit for amplitude variation stated in the document is the radar loop gain (RLG). RLG includes both transmitter and receiver gain of the radar.

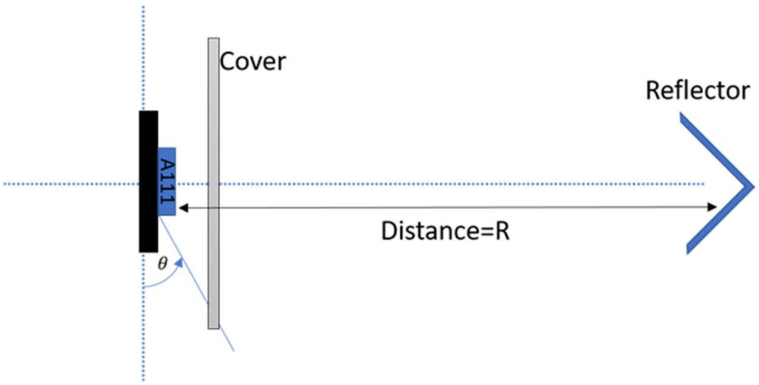

Figure 4. Measurement setup for radar loop gain radiation pattern.

3.3 PCB layout

This chapter describes means of optimizing the sensor performance by properly designing the printed circuit board (PCB).

3.3.1 Sensor ground plane size

To maximize the radar loop gain and minimize impact on radiation pattern, it is recommended that the top PCB layer is a filled copper layer with minimum amount of routing close to the sensor. Figure 5 shows the relative loss in RLG as a function of ground plane size, assuming a solid square ground plane and the sensor placed at the center. As the ground plane size is increased, the RLG increases because of increased antenna directivity. However, the RLG doesn't increase monotonically with ground plane size due to constructive and destructive interference.

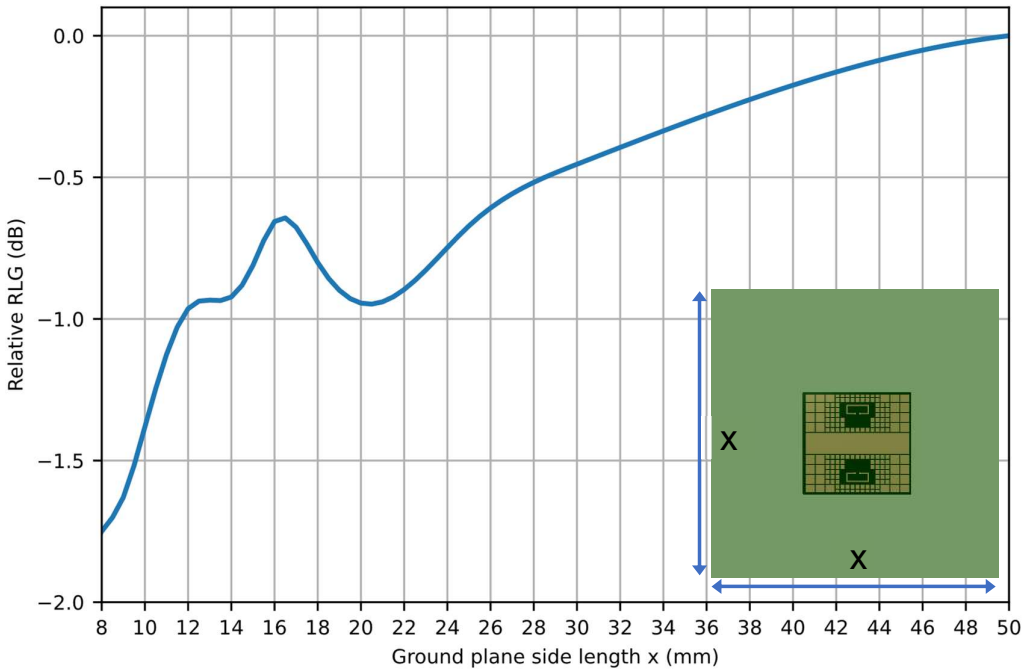

Figure 5. Simulated relative radar loop gain as a function of ground plane side length (x). Ground plane is a solid square ground plane without routing.

In terms of regulatory compliance, any openings in the ground plane inside the A111/A121 BGA footprint must be significantly smaller than the wavelength of the radiation that is being blocked, to effectively approximate an unbroken conducting surface.

3.3.2 Impact of PCB routing and nearby components

As no RF components are required for the sensor integration, low-cost FR-4 type PCBs can generally be used. However, for a symmetrical RLG pattern and maximum directivity, the following PCB design rules should be considered:

- Whenever possible, place decoupling capacitors and the crystal on the opposite side of the PCB. In other cases, the decoupling capacitors can be placed as in Figure 6b and the crystal placed some distance away from the sensor. A small RLG loss of approximately 0.5 dB is seen when placing decoupling capacitors (metric 1005 or smaller) as shown in Figure 7.
- Minimize amount of routing close to the sensor. This can be done by routing the signals to the sensor with vias placed as close as possible to the sensor pads as shown in Figure 6. The ground plane area

inside the footprint has lower impact on the radiated performance and therefore some vias and short traces are preferably placed there while still satisfying regulatory compliance.

- Minimize copper clearance for traces, vias and pads on the sensor layer.
- If the PCB assembly process allows, connect all ground pads without thermal reliefs as shown in Figure 6a-b. This can increase the boresight RLG by approximately 1.5 dB compared to Figure 6c, provided there are no other interfering components or PCB traces close to the sensor, see Figure 7.

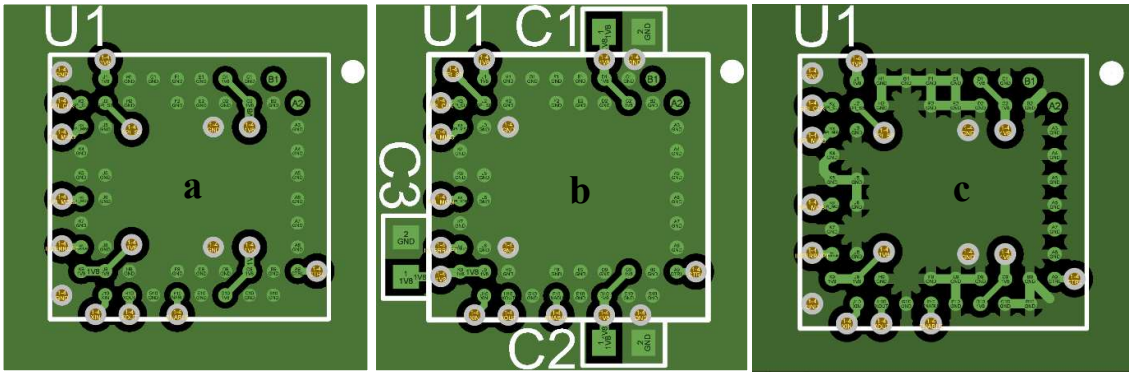

Figure 6. A111 routing examples with vias placed close to sensor for maximizing ground plane size. (a) Without GND thermal reliefs, (b) with decoupling capacitors and without GND thermal reliefs, (c) with GND thermal reliefs. Trace to copper clearance is 0.127 mm.

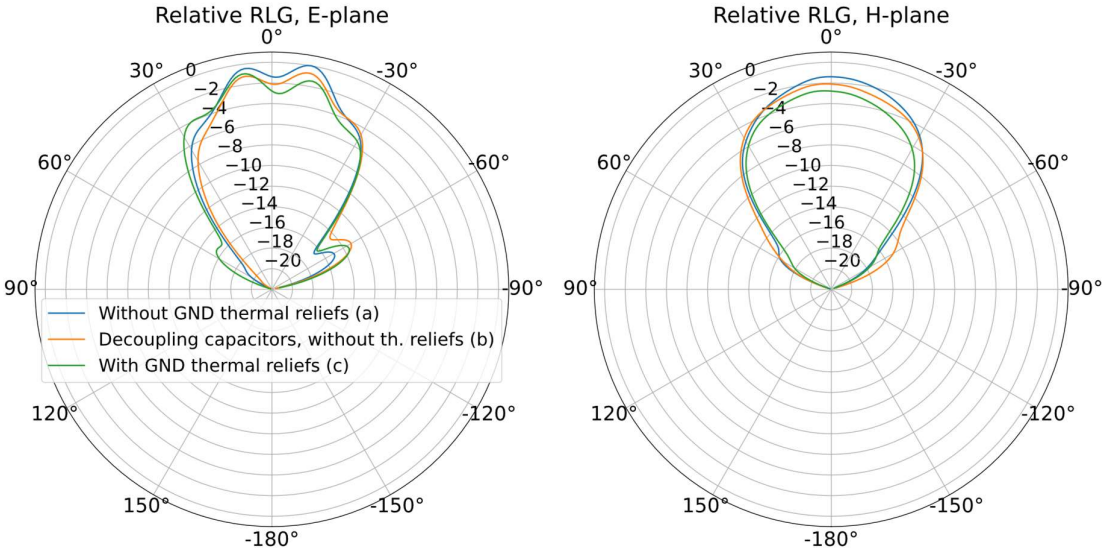

Figure 7. Relative RLG loss with and without A111 thermal reliefs.

Example PCB designs can be found on the Acconeer developer page [1].

For designs requiring larger components close to the sensor, a tapered shielding wall can be designed as shown in Figure 8.

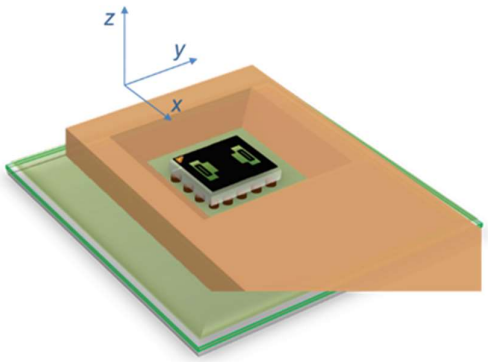

Figure 8. Tapered shield wall designed to prevent unwanted reflections from components placed close to the radar sensor.

3.4 Impact of conformal coating

Conformal coating may be used to protect the sensor and other electronic components from environmental factors such as moisture, dust, and chemicals. Conformal coatings are typically made of polymeric materials with dielectric constants typically in the range $\varepsilon_r < 4$. Depending on the coating material properties and layer thickness, one can expect a drop in the sensor's radar loop gain (RLG). This gain drop is due to three factors;

1. Offset in antenna resonance frequency as the antenna becomes electrically longer.
2. Reflection and refraction loss due to the interface between the sensor and the coating.
3. Dielectric loss in the coating material. This can usually be neglected for thin coating layers (e.g. <200 µm).

Figure 9 shows the simulated relative radar loop gain (RLG) after a linear lossless ($\tan(\delta) = 0$) isotropic coating has been added to all sides of the radar sensor. As the coating thickness increases and/or the dielectric constant increases, the RLG decreases. The loss is however non-monotonic, and this is due to constructive and destructive interference depending on the coating thickness.

The loss due to antenna resonance frequency offset can be seen in Figure 10 where the maximum gain is shifted in frequency. This means that, as the radar signal is a wideband signal, the resulting loss in SNR can be expected to be somewhat less than what is estimated in Figure 10.

If it is critical to obtain the maximum gain, it is recommended to use a thin coating layer (< 40 µm) with low dielectric constant and loss factor. However, as many coating materials are not well characterized at mm-wave frequencies it may be best analyzed by performing actual tests.

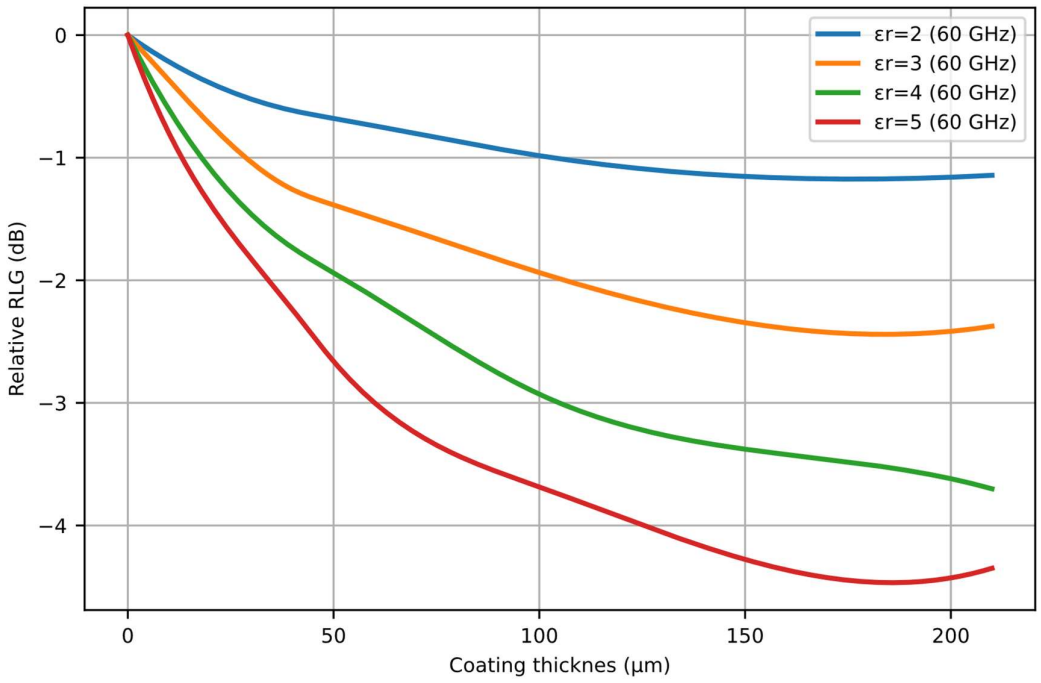

Figure 9. Simulated impact of lossless dielectric conformal coating on radar loop gain (RLG) at 60 GHz.

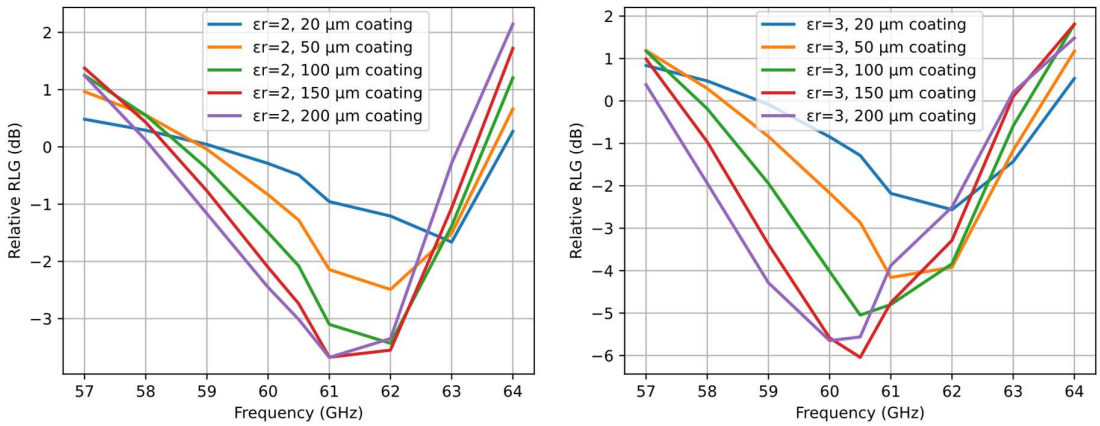

Figure 10. Simulated impact of conformal coating with εr =2 and εr =3 for different thicknesses.

3.5 Sensor underfill

Underfills can be used to fill the gap between the sensor package and PCB. The sensor underfill material should be chosen to have as low dielectric constant and loss tangent as possible. Dielectric constant determines the reflectivity of the medium and loss tangent indicates the dissipation effect of the material and both are frequency dependent.

3.6 Electromagnetic propagation

The following concepts are important for understanding how the radar can be properly integrated into product encapsulations.

3.6.1 Transmission and reflection

When an electromagnetic (EM) wave hits the interface between two dielectrics, reflection and refraction take place at the boundaries. Inside the dielectric, the propagation speed and wavelength changes depending on the material permittivity. If the wavelength in free space is λ_0, the wavelength within the material is $\lambda_0/\sqrt{\epsilon_r}$, where ϵ_r is the relative dielectric constant of the material.

In the case of linearly polarized propagation at normal incidence, the Fresnel equations then relate the ratio between the incident and transmitted fields [5]:

$$r = \frac{Z_2 - Z_1}{Z_2 + Z_1}, t = \frac{2Z_2}{Z_2 + Z_1}, \tag{3}$$

where Z_1 and Z_2 are the corresponding wave impedances. We can also calculate the transmission factor from $t = 1 + r$. In most cases we have non-magnetic materials so that $Z = \sqrt{\mu_r/\epsilon_r} = 1/\sqrt{\epsilon_r}$. An important special case is normal incidence between air and dielectric. The reflection coefficient then simplifies to

$$r = \frac{1 - \sqrt{\epsilon_r}}{1 + \sqrt{\epsilon_r}}$$

It is immediately obvious that the higher the dielectric constant, the stronger the reflected signal. Conductors have a high dielectric constant ($\epsilon_r \to \infty$) and will therefore give a strong reflection. Most polymers have a dielectric constant in the range of 2 – 4 and will therefore give a weaker reflection.

3.7 Radomes

A radome is a dielectric layer that is transparent to the radar signal while protecting the radar from mechanical impact and weather, see Figure 11. Often the product encapsulation can be made as a radome without introducing additional costs. We will here see that by tuning the radome thickness and distance, the radome can be made transparent to the radar.

3.7.1 Radome thickness

Let d_1 be the distance to the radome, d_2 the thickness, r_1 and r_2 the reflection coefficients and t_1 and t_2 the corresponding transmission coefficients, see Figure 11. As an incident wave hits the first interface, a reflection r_1 and transmission t_1 happens. Notice that $r_1 < 1$ so that the reflected wave is out of phase with the incident wave. At the second interface, another reflection (r_2) and transmission takes places (t_2). With air on both sides of the dielectric, we note from Eq. (3) that $r_1 = -r_2$. The *total* reflection coefficient Γ_1 then becomes [5]

$$\Gamma_1 = \frac{r_1(1 - e^{-2jkd_2})}{1 - r_1^2 e^{-2jkd_2}},$$

where $k = 2\pi/\lambda$ is the wave number in the material. Two important special cases follow:

For $d_2 = m\frac{\lambda}{2}, m = 1,2,\ldots$ we have e^{-2jkT}=1 or $\Gamma_1 = 0$ (4)

For $d_2 = m\frac{\lambda}{4}, m = 1,3,5,\ldots$ we have e^{-2jkd_2}=-1 or $\Gamma_1 = 2r_1/(1 + r_1^2)$. (5)

The optimum radome thickness, that is, the dielectric is perfectly reflectionless for thicknesses equal to a multiple of half a wavelength. This can also be understood from that the round trip of the wave inside the radome (t_1) introduces a 360-degree phase shift therefore cancelling out the reflected wave r_1.

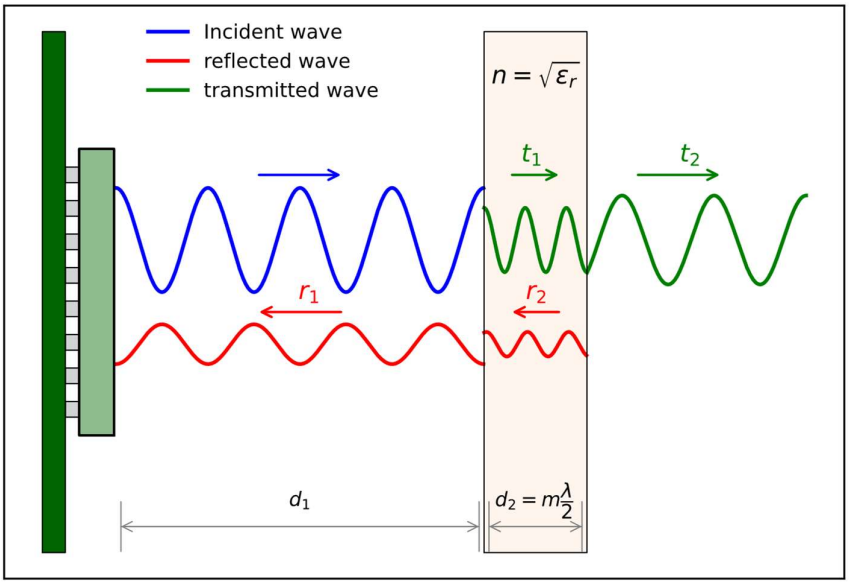

Figure 11. Transmitted and reflected signals from a half wavelength radome. Secondary reflections have been omitted for simplicity.

As an example, if the material relative permittivity is $\epsilon_r = 2.6$, the optimal radome thickness becomes

$$d = m\frac{\lambda}{2} = m\frac{\lambda_0}{2\sqrt{\epsilon_r}} = m\frac{5}{2\sqrt{2.6}} = m * 1.55 \text{ mm}$$

If the dielectric is an odd multiple of $\lambda/4$, we encounter maximum reflection.

3.7.2 Radome distance

In addition to the radome thickness, the distance between the sensor and radome impacts. Depending on the radome thickness and distance, the initial reflection from the radome will further cause multiple reflections from the sensor, PCB and radome. This leads to a standing wave pattern where the amplitude varies as a function of the radome distance. The amplitude variation will be a minimum if the reflected wave from the radome is in-phase with the transmitted wave, that is, the optimum radome distance is

$$d_1 = m\frac{\lambda_0}{2}, m = 1, 2, 3, \ldots$$

This optimum distance is valid if the thickness of the radome is optimum as well. In the case when this cannot be fulfilled, minimum insertion loss on the received signal is obtained when the distance to the sensor satisfies the following criteria:

$$m\frac{\lambda_0}{4} - \delta < d_1 < m\frac{\lambda_0}{4} + \delta, m = 1, 3, 5, \ldots$$

In order to have zero insertion loss, δ is determined to be 0.5 mm.

Figure 12 shows the amplitude variation as a function of distance d_1 with a 1 mm thick radome made of ABS (ϵ_r=2.6). When the distance d_2 gets larger than the pulse length, the standing wave disappears.

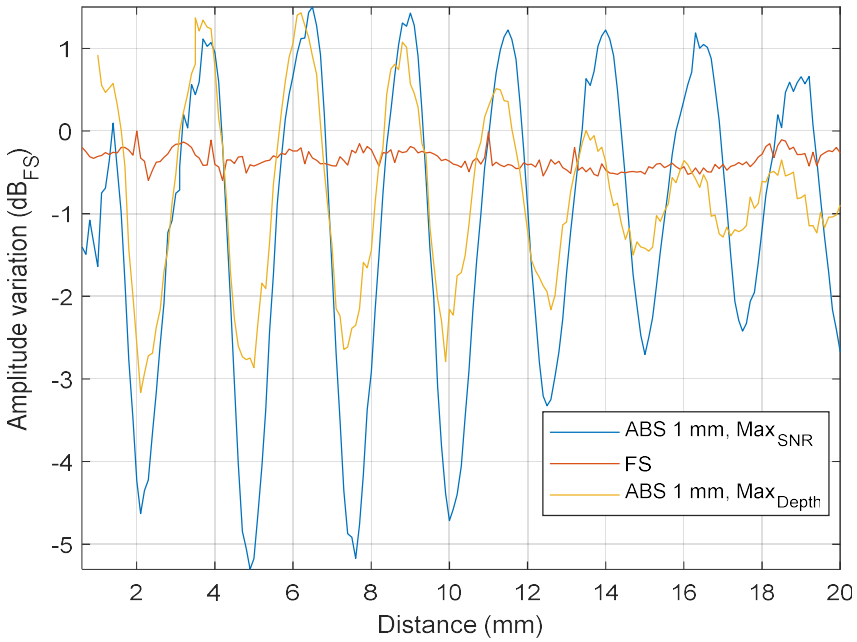

Figure 12. Measured reflected power from the target versus the 1 mm radome to sensor distance for two different profiles. Amplitude is normalized by the free space amplitude for each profile. Amplitude variation is stated in one direction (Tx or Rx side). For Radar loop Gain (RLG) the values will be doubled.

Figure 13 shows the measured amplitude variation of the reflected wave from a radar target when the distance between the sensor and the radome is varied for different radome thicknesses. A radome thickness of λ/2 = 1.6 mm results in the smallest amplitude variation whereas as thickness of λ/4 = 0.7 mm gives the largest amplitude variation.

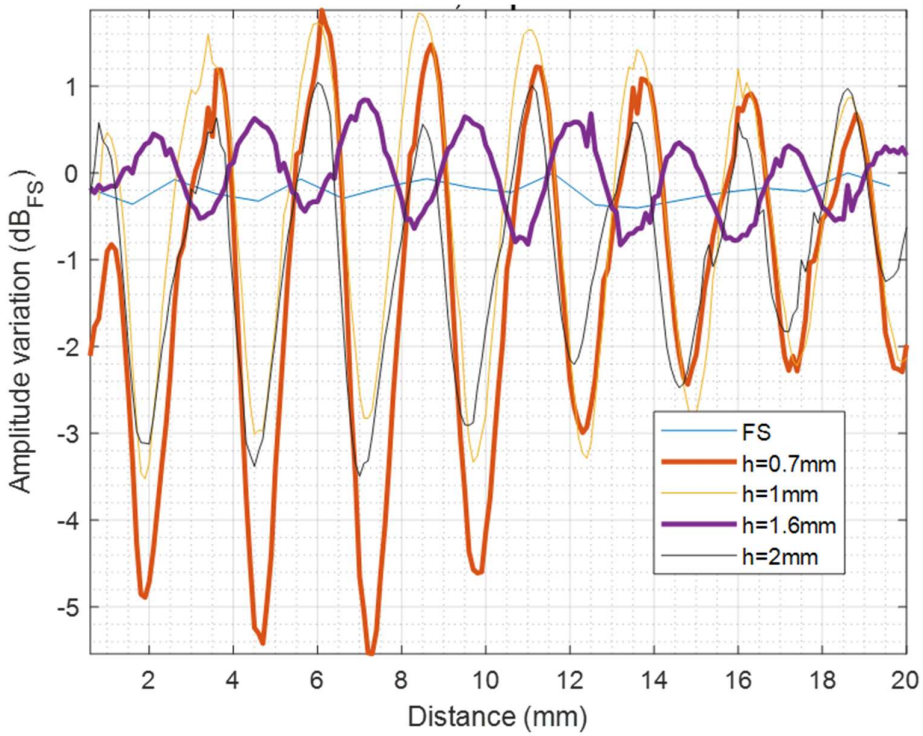

Figure 13. Impact of the thickness of the radome (made of ABS) on the reflected amplitude variation. The amplitude is normalized to maximum value of the free space (FS). Amplitude variation is stated in one direction (Tx or Rx side). For Radar Loop Gain (RLG) the values will be doubled.

If absolute measurements are required for a certain use case, it is advised that an additional offset is added to the distance measurement. The reason for this offset is that the propagation delay caused by the radome must be compensated. This additional offset is obtained by making reference measurements, and it will also allow you to place the reference plane at the desired location for your product. For multi-layer radome optimization, readers can find more information in [5].

3.7.3 Impact of radome on the RLG pattern

Figure 14 and Figure 15 shows the radar RLG pattern when a radome made of ABS with a permittivity of $\varepsilon_r = 2.6$, with *λ/2* (1.6 mm) and *3λ/4* (2.2 mm) thickness is placed at distances corresponding to the harmonics of the quarter-of-a-wavelength of the radar pulse. The reference case is FS (free space i.e. no radome). For the case of an optimal thickness, 1.6 mm, the variation because of the distance is minimized. λ_0 is the free space wavelength at 60.5 GHz, 5 mm. λ is the wavelength in the dielectric at 60.5 GHz, in this case, 3.1 mm. The reason for the increased gain of the *3λ/4* (2.2 mm) radome compared to free space is because of constructive interference from the reflected wave at the sensor.

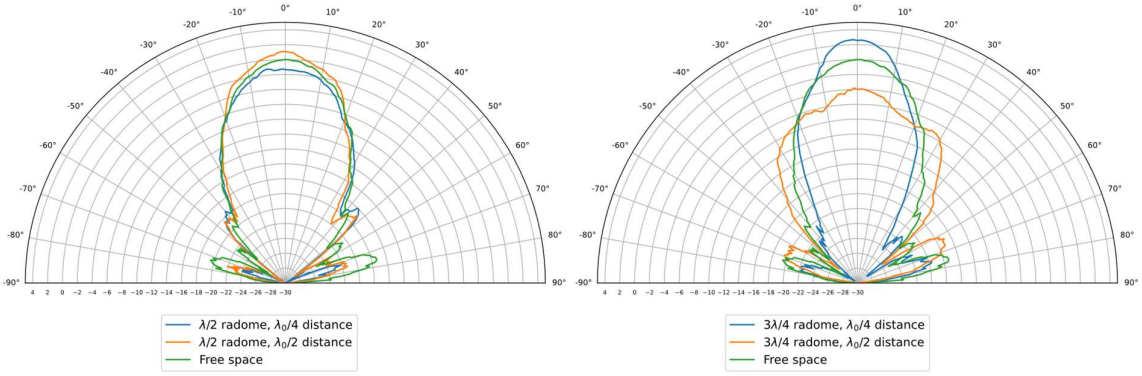

Figure 14: Impact of the radome-to-sensor distance on the RLG pattern (E-plane). The radial axis is the amplitude, stated in two directions (Tx and Rx side), i.e. Radar Loop Gain (RLG) and normalized to free space radiation.

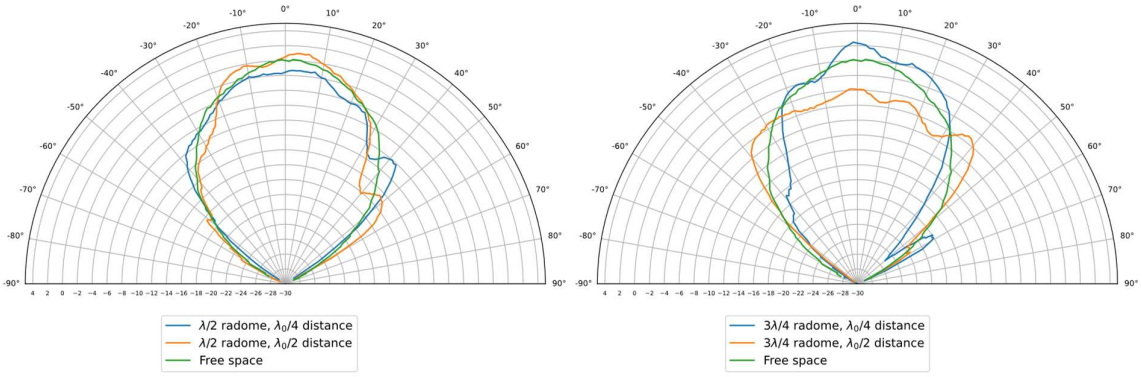

Figure 15: Impact of the radome-to-sensor distance on the RLG pattern (H-plane). The radial axis is the amplitude, stated in two directions (Tx and Rx side), i.e. Radar Loop Gain (RLG) and normalized to free space radiation.

It is not recommended to place the cover directly on the sensor. Figure 16 shows the RLG pattern on the E- and H-plane when the cover (ABS plastic sheet) is located on top of the sensor. In comparison with free space, there is around 6 dB loss on both max. power and total radiated power for this case.

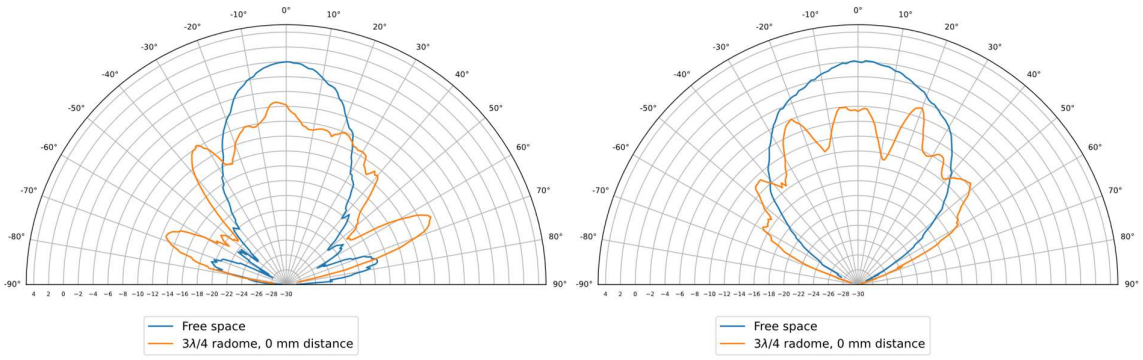

Figure 16: RLG pattern of E-plane and H-plane, cover placed directly on the sensor vs free space. The radial axis is the amplitude, stated in two directions (Tx and Rx side), i.e. Radar Loop Gain (RLG) and normalized to free space radiation.

4 Dielectric lenses

Dielectric lenses are a cost-effective way of shaping the radiation patterns, especially for millimeter wave applications where the size of the lens becomes small enough. Although it is most common to design lenses for increasing the gain and to narrow the beamwidth, lenses can also be used for increasing the beamwidth, tilted beams as well as to suppress side lobes to reject unwanted reflections.

Since many common thermoplastics used in product design also have low permittivity and low loss, a lens can often be incorporated into the same encapsulation material with little additional cost. 3D printing technology allows for rapid prototyping and can often resemble the performance of the final product. Dielectric lenses are also more compact and cheaper to fabricate than corresponding horn antennas and reflectors.

To quickly get started using a lens, Acconeer provides two example lenses, one plano-convex and one FZP type lens, see Figure 17. Both lenses can be used with all module evaluation kits. The FZP lens is similar to the example lens in Ch. 4.3.1. The user guide and performance of these lenses can be found in [6].

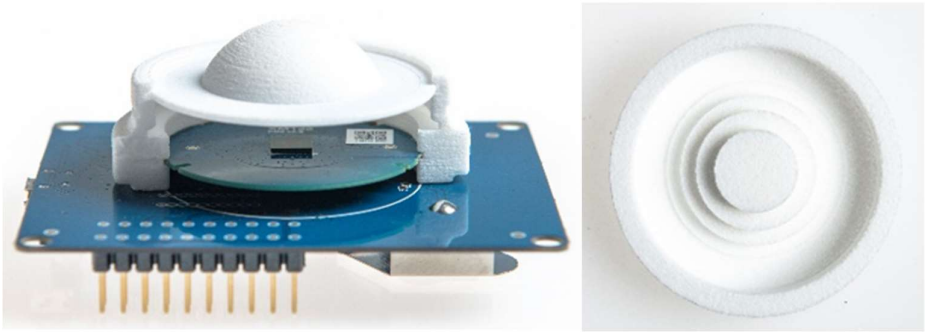

Figure 17. Plano-convex (left) and Fresnel Zone Plate lens (right) from Acconeer lens kit [6].

4.1 Refracting lenses

4.1.1 Design principles

Figure 18a shows a spherical wavefront from the A111/A121 sensor feeding a converging lens of refractive index $n = \sqrt{\epsilon_r}$. The lens refracts the spherical waves to produce parallel waves for increasing the directivity. Figure 18b shows the corresponding ray optics model where rays propagate from the source as diverging straight lines until hitting the first surface and refracting into parallel rays. Ray optics doesn't account for interference, diffraction, and polarization but it does give us a basic understanding of dielectric lenses, and most importantly, allows us to quickly construct analytical lens shapes for many applications.

In the following we assume that all lens profiles are axial symmetric, although asymmetrical lenses can be designed for customized radiation patterns. For a converging lens, two criteria need to be fulfilled: (1) Refraction at one or both surfaces to produce parallel rays at the output, and (2), the rays just outside the outer surface have to be coherent (in-phase). One of the lens surfaces can be chosen arbitrarily, for example planar or spherical. Next, we will provide design equations for constructing converging lenses fulfilling these criteria.

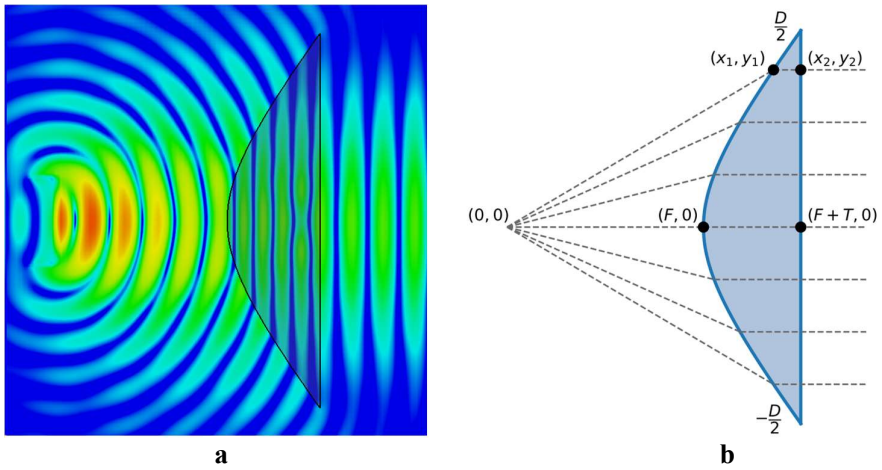

Figure 18. Hyperbolic lens with spherical E-field source (a) and corresponding ray model (b).

4.1.2 Convex-planar lens (Hyperboloidal lens)

By constraining the outer surface to planar we have $x_2 = F + T$, see Figure 18b. Equating the optical path through a point (x_1, y_1) with the central path yields

$$\sqrt{x_1^2 + y_1^2} = nx_1 + (1 - n)F. \tag{6}$$

Eq. (6) can be written as

$$\left(\frac{x_1 - x_0}{a}\right)^2 - \left(\frac{y_1}{b}\right)^2 = 1, \tag{7}$$

where the coefficients are given by

$$a = \frac{F}{n+1}, b = \sqrt{\frac{n-1}{n+1}}F, x_0 = \frac{nF}{n+1}.$$

Observe that we have refraction only at the inner surface, that is, this is a single refracting lens. We recognize Eq. (7) as a hyperbolic function shifted in the x direction by x_0, hence the name hyperbolic (2D) or hyperboloidal (3D) lens.

The central thickness of the lens can be shown to be

$$T = \frac{1}{n+1}\left(\sqrt{F^2 + \frac{(n+1)D^2}{4(n-1)}} - F\right). \tag{8}$$

To generate a lens profile, we first choose a material $n = \sqrt{\epsilon_r}$. After this the diameter D and the focal distance F is chosen to fulfill some maximum thickness requirement in Eq. (8). The lens profile is then given by Eq. (7) by solving for $y_1 = y_1(x_1), x_1 \in [F, F + T]$. A parametrization $\left(x_1(t), y_1(t)\right)$ may be required for generating the lens profile in CAD software. One such parametrization is

$$\begin{cases} x_1 = x_0 + a\sqrt{1+\left(\frac{t}{b}\right)^2}, t \in \left[-\frac{D}{2}, \frac{D}{2}\right] \\ y_1 = t \end{cases}$$

4.1.3 Plano-convex lens

Constraining the inner surface to planar results in a plano-convex lens, see Figure 19. We then have $x_1 = F$ and carrying out the algebra results in the following parametric solution for the outer surface:

$$\begin{cases} x_2 = \dfrac{\left((n-1)T - \sqrt{F^2+y_1^2}\right)\sqrt{(n^2-1)y_1^2+n^2F^2} + n^2F\sqrt{F^2+y_1^2}}{n^2\sqrt{F^2+y_1^2} - \sqrt{(n^2-1)y_1^2+n^2F^2}} \\ y_2 = y_1\left(1 + \dfrac{x_2 - F}{\sqrt{(n^2-1)y_1^2+n^2F^2}}\right) \end{cases} \quad (9)$$

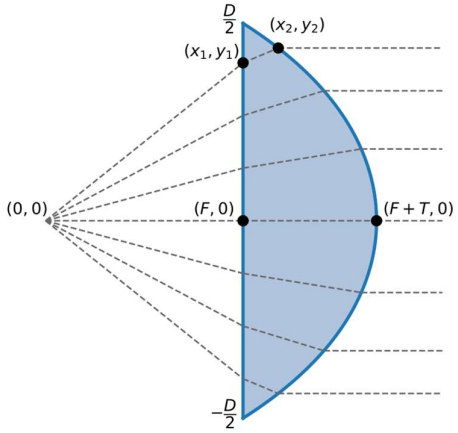

Figure 19. Plano-convex lens ray model.

The central thickness is given by

$$T = \frac{\sqrt{4F^2+D^2} - 2F}{2(n-1)}.$$

Contrary to the hyperboloidal lens, we now have refraction at both the inner and the outer surfaces. The lens profile given in Eq. (9) do not resemble any known function and we therefore simply call this lens a plano-convex lens.

4.2 Lens gain

The lens gain is related to the lens effective area by $G = 4\pi A_e/\lambda^2$, where λ is the wavelength in the material. Approximating the effective area with the lens inner surface area $A_e = \pi(D/2)^2$, we obtain $G = \pi^2 D^2/\lambda^2$. We thus notice that the lens gain is proportional to the square of the diameter. To get the lens RLG, we double the lens gain.

Figure 20 and Figure 21 show simulated RLG pattern plots for the hyperbolic and the plano-convex lenses for some sample values of F and D. These figures can be used as a rough guideline for choosing the lens size. Observe that for the same diameter, the plano-convex lens yields somewhat higher gain compared to the hyperbolic lens. The exact RLG pattern will also depend on the lens housing, choice of material and PCB size.

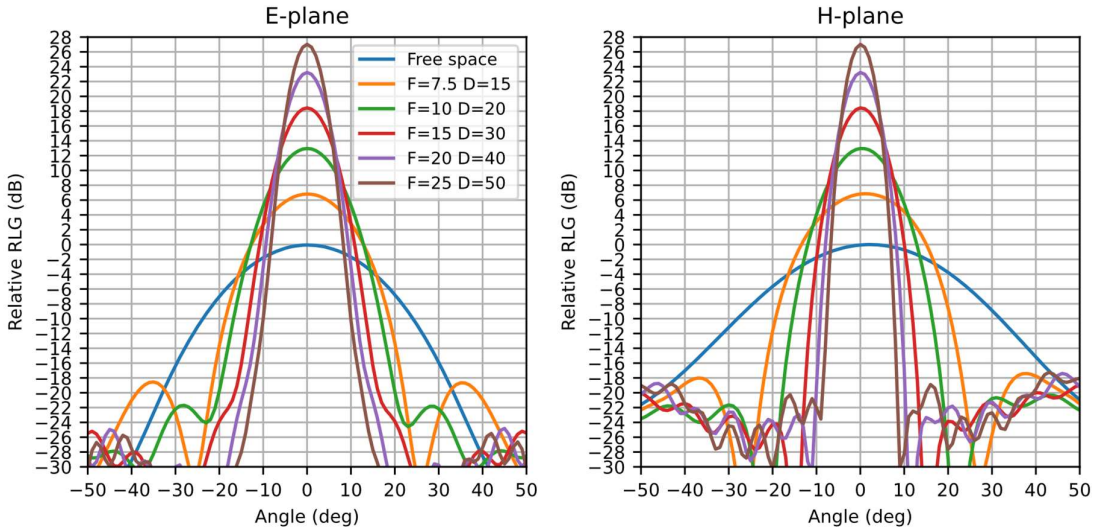

Figure 20. Simulated RLG patterns for different size hyperbolic lenses assuming lossless dielectrics.

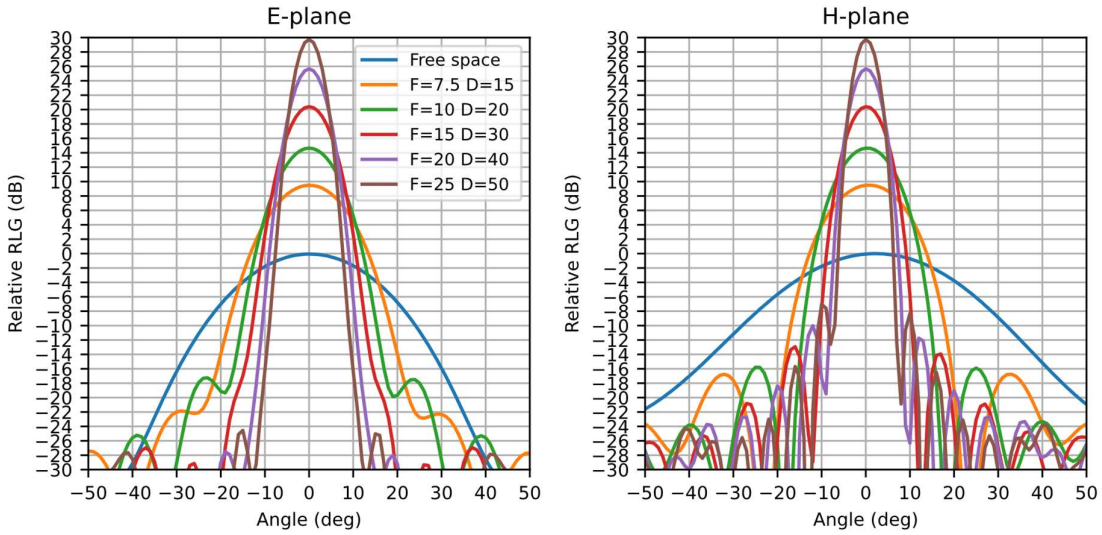

Figure 21. Simulated RLG patterns for different size plano-convex lenses assuming lossless dielectrics.

4.3 Fresnel Zone Plate (FZP) lenses

The plano-convex and convex-planar type lenses are refracting type lenses. Another popular lens type is the Fresnel zone plate lens which is based on diffraction instead of refraction [7]. Different types of FZP lenses exists and here the phase correcting FZP lens is covered. The FZP lens structure is composed of dielectric rings with different thickness for correcting the phase of the incident waves. Figure 22 shows an example of FZP lens consist of 3 zones with the phase step of quarter of wavelength.

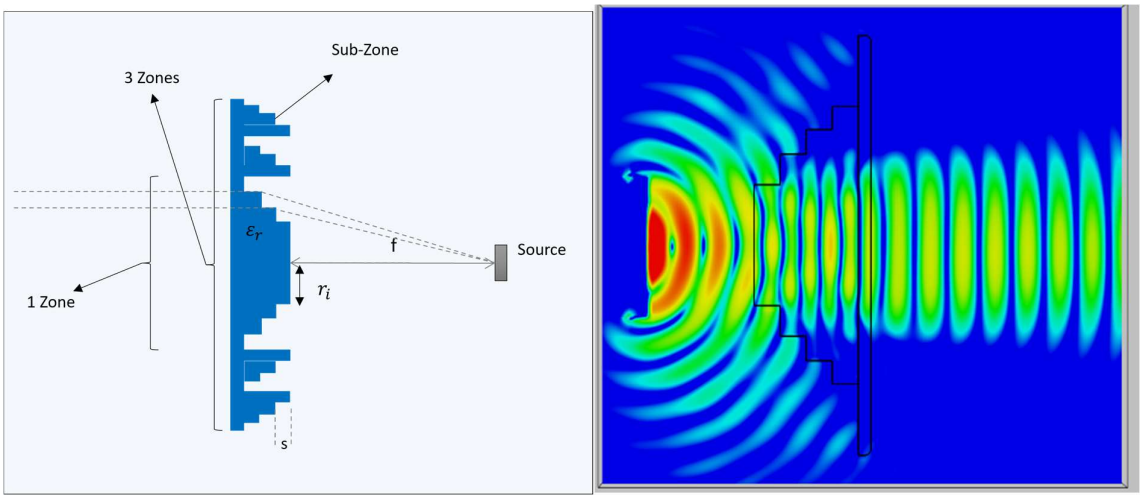

Figure 22. FZP lens, collimating the beam originating from the source at distance f (focal length)

The radius r_i of the rings and the step thickness s can be calculated from Eqs. (10) and (11)

$$r_i = \sqrt{2Fi\frac{\lambda}{P} + \left(\frac{i\lambda}{P}\right)^2}, i = 1, \dots N \tag{10}$$

$$s = \frac{\lambda}{P(\sqrt{\epsilon_r} - 1)} \tag{11}$$

Here F is the focal point, P is the number of sub-zones or steps, λ is the wavelength in free space (5 mm at 60 GHz), and ε_r is the relative dielectric constant. For small diameter lenses, we can choose one zone and 4 or 8 steps. For larger diameter lenses, additional sub zones can be added for increased gain. Notice that contrary to the refracting type lenses, the ring thickness and hence the lens total thickness is independent of the lens radius. This allows us to construct large diameter lenses without increasing the thickness.

4.3.1 Example FZP lens calculation

This is an example of a single zone FZP lens with a focal point F=10 mm and quarter of wavelength steps or N=4. We assume a material permittivity of $\varepsilon_r = 2.6$. Inserting this into Eq. (10) gives us the lens radii as follows:

$r_1 = 5.1$ mm, $r_2 = 7.46$ mm, $r_3 = 9.39$ mm, $r_4 = 11.12$ mm

Eq. (11) gives us the step thickness of s= 2.02 mm. Total thickness of the lens is then 4*2.02 = 8.1 mm.

For further details regarding FZP lens design, see [7].

4.3.2 Lens thickness comparison

For mass production, injection molding is usually cost effective but producing thick lenses can be challenging as sink marks and other deformations can occur. It is therefore of interest to find lens designs which are as thin as possible. In Figure 23 we have compared the lens thickness to diameter ratio (T/D) as a function of ε_r. Common thermoplastics have ε_r in the range 2-4 and the hyperboloidal lens is the thinnest lens. To further obtain thinner lenses we can increase the F/D ratio, but this may also increase the side lobe level due to spillover radiation from the sensor, especially for small diameter lenses.

Smaller F/D ratios can be chosen than 0.5 with the cost of increased thickness. For short focal distance lenses, the FZP lens is a good option as its thickness only depend on ε_r.

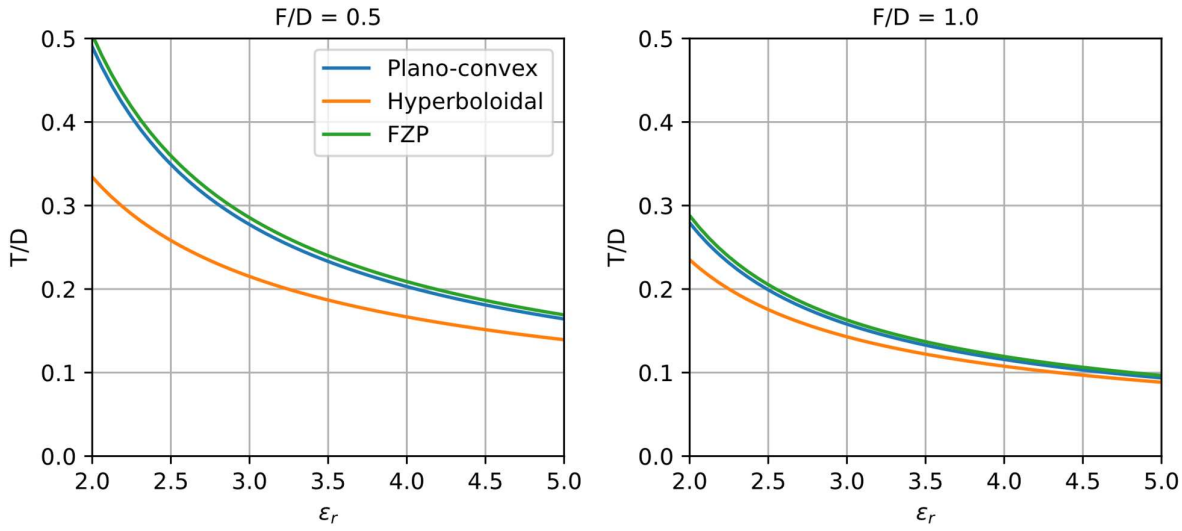

Figure 23. Lens thickness comparison.

4.4 Lens design guidelines and prototyping

In general, multiple design aspects must be considered when choosing a lens type. Whenever possible, the lens can be made as a part of the outer enclosure and therefore avoid the need for an additional radome. For applications requiring a flat outer surface, convex-planar or FZP lenses are good choices. Outdoor applications may need to consider rain or ice buildup and here the lens outer surface is chosen to minimize this impact. For example, an upwards pointing convex surface would collect less rain.

Manufacturing lenses by injection molding may pose limitations on the lens maximum thickness. For the refracting type lenses, thin lenses are obtained by choosing a high F/D ratio and higher permittivity materials. On the other hand, higher F/D ratios occupy more space as well as increased spillover energy which in turn leads to larger side lobes. For the plano-convex and convex-planar lenses, it is therefore recommended to keep $0.4 < F/D < 0.8$. Lens designs with F/D outside this range is certainly possible, but with additional loss in directivity and increased side lobes. When large diameter lenses are required, FZP type lenses should be considered as its thickness only depend on the permittivity and are thus generally thinner than refracting type lenses.

For maximum gain and low side lobe level, it is important to also follow the PCB ground plane guidelines in Chapter 3.3.

4.4.1 Focal distance tuning

The focal distance *F* is an input parameter for all lens designs provided here. However, the optimal focal distance may need to be slightly adjusted such that the reflection from the lens is simultaneously minimized. In addition, other effects can impact the focal point, such as material permittivity being slightly off, impact of lens housing, radomes and other nearby mechanics.

Figure 24 shows the gain variation of the integrated lens with the radome with respect to the free space scenario for the XM112 module. The maximum gain happens at 7.5 mm distance for both lenses. Other maxima happen every half-a-wavelength (2.5 mm).

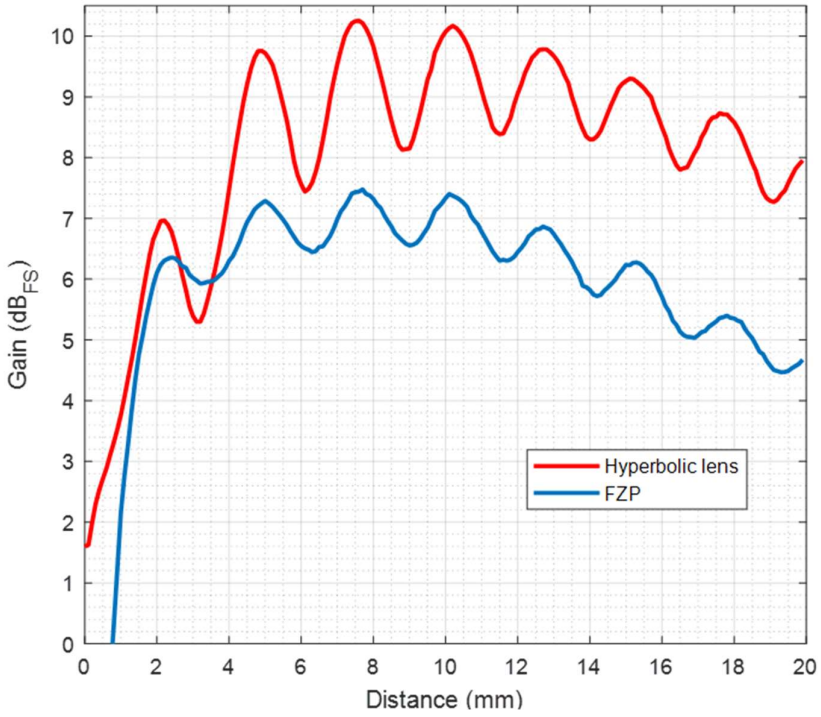

Figure 24. Gain variation of the lens versus the distance to the XM112 radome. The amplitude is normalized to free space (FS). Gain is stated in one direction (Tx or Rx side). For Radar Loop Gain (RLG) the values will be doubled.

4.4.2 Customized lenses

The lens design equations provided here are based on ray optics and may not be adequate in more challenging applications, especially when the lens diameter is small. With a full wave EM solver, Acconeer can construct optimized lenses for maximizing the gain, minimizing side lobes or customizing radiation patterns. The impact of lens housings, nearby mechanics and the PCB can also be simulated. Acconeer provides a design service for this, visit the Acconeer Developer page for details [1].

5 References

[1] "Acconeer developer page," [Online]. Available: https://developer.acconeer.com.

[2] Acconeer, "A111 datasheet," [Online]. Available: https://developer.acconeer.com/download/a111-datasheet-pdf.

[3] Acconeer, "A121 datasheet," [Online]. Available: https://developer.acconeer.com/download/a121-datasheet-pdf/.

[4] Acconeer, "Handbook," [Online]. Available: https://docs.acconeer.com/en/latest/handbook.

[5] S. J. Orfanidis, Electromagnetic Waves and Antennas, New Jersey: Rutgers University, 2016.

[6] Acconeer AB, "Getting Started Guide Lenses," [Online]. Available: https://developer.acconeer.com/download/getting-started-guide-lenses-pdf.

[7] J. C. W. D. N. Black, "Millimeter-Wave Characteristics of Phase-Correcting Fresnel Zones Plates," *IEEE Transactions on microwave theory and techniques,* vol. 35, no. 12, 1987.

[8] S. R. Artem Boriskin, Aperture Antennas for Millimeter and Sub-Millimeter Wave Applications, Springer, 2017.

[9] K.-C. H. John Thornton, Modern Lens Antennas for Communications Engineering, Wiley-IEEE Press, 2013.

[10] "Acconeer Expolration Tool," [Online]. Available: https://acconeer-python-exploration.readthedocs.io/en/latest/sensor_introduction.html.

[11] "Acconeer PCR sensor A111 EVK hardware userguide," [Online]. Available: https://developer.acconeer.com/download/xc112_xr112-user-guide-pdf.

[12] T. Milligan, Modern Antenna Design, 2nd Edition, Wiley & Sons, 2005.

[13] E. Hecht, Optics, 5th Edition, Pearson Education, 2017.

[14] G.-A. e. al, "Analytical Lens Design," 2020. [Online]. Available: https://iopscience.iop.org/book/mono/978-0-7503-3167-8.

[15] F. e. al, "Dielectric Lens Antennas (Pre-print)," [Online]. Available: https://repositorio.iscte-iul.pt/bitstream/10071/11959/1/pre_print_Dielectric_Lens_Antennas_v2.pdf.

[16] S. L. Y. T. Lo, Antenna Handbook, volume II, Thomson Publishing, 1993.

6 Appendix A: Materials

Table 1. Measured dielectric constant and loss tangent of different materials at 60 GHz [8].

Material	Dielectric constant	Loss tangent
ABS-M30 (three-dimensional printed)	2.48	0.008
Acrylic glass	2.5	0.0118
Alumina	9.3	0.0013
Fused quartz	3.8	0.0015
MACOR	5.5	0.0118
PLA (three-dimensional printed)	2.85	0.014
Polyethylene	2.3	0.0003
Polypropylene	2.2	0.0005
Polystyrene (Rexolite)	2.5	0.0004
Teflon	2.2	0.0002

7 Revision

Date	Version	Changes
2019-11-13	1.0	Original version
2020-07-02	1.2	Comments on the gain values
2020-11-25	1.3	Added information about conformal coating. Updated pictures of GND planes in chapter 3.
2022-03-07	1.4	Updated chapter 3 on PCB routing.
2022-03-08	1.5	Fixing formatting issues
2023-03-30	1.6	Updates for A121 sensor. Added chapter on dielectric lens design.
2024-02-07	1.7	Fixed typo in Eq. (9). Updated Figure 11. Corrected Equation (11) has therefore been corrected.

Disclaimer

The information herein is believed to be correct as of the date issued. Acconeer AB (“**Acconeer**”) will not be responsible for damages of any nature resulting from the use or reliance upon the information contained herein. Acconeer makes no warranties, expressed or implied, of merchantability or fitness for a particular purpose or course of performance or usage of trade. Therefore, it is the user’s responsibility to thoroughly test the product in their particular application to determine its performance, efficacy and safety. Users should obtain the latest relevant information before placing orders.

Unless Acconeer has explicitly designated an individual Acconeer product as meeting the requirement of a particular industry standard, Acconeer is not responsible for any failure to meet such industry standard requirements.

Unless explicitly stated herein this document Acconeer has not performed any regulatory conformity test. It is the user’s responsibility to assure that necessary regulatory conditions are met and approvals have been obtained when using the product. Regardless of whether the product has passed any conformity test, this document does not constitute any regulatory approval of the user’s product or application using Acconeer’s product.

Nothing contained herein is to be considered as permission or a recommendation to infringe any patent or any other intellectual property right. No license, express or implied, to any intellectual property right is granted by Acconeer herein.

Acconeer reserves the right to at any time correct, change, amend, enhance, modify, and improve this document and/or Acconeer products without notice.

This document supersedes and replaces all information supplied prior to the publication hereof.